PHYSICAL REVIEW D

PARTICLES AND FIELDS

THIRD SERIES, VOLUME 41, NUMBER 7 1 APRIL 1990

Quark hadronization probed by K^0 mesons

S. Abachi,[a] M. Derrick, P. Kooijman,[b] B. Musgrave, L. Price, J. Repond, and K. Sugano
Argonne National Laboratory, Argonne, Illinois 60439

D. Blockus,[d] B. B. Brabson, J.-M. Brom,[c] C. Jung,[d] H. Ogren, D. R. Rust, and A. Snyder[d]
Indiana University, Bloomington, Indiana 47405

B. Cork
Lawrence Berkeley Laboratory, Berkeley, California 94720

C. Akerlof, J. Chapman, D. Errede,[e] M. T. Ken, P. Kesten,[f] D. I. Meyer, H. Neal, D. Nitz, R. Thun, and R. Tschirhart[a]
University of Michigan, Ann Arbor, Michigan 48109

P. Baringer,[g] B. G. Bylsma,[h] R. Debonte, E. H. Low,[i] R. L. McIlwain, D. H. Miller, C. R. Ng, K. Rangan,[j] and E. Shibata
Purdue University, West Lafayette, Indiana 47907

(HRS Collaboration)

(Received 2 August 1989)

Total and differential K^0 cross sections are presented from e^+e^- collisions at $\sqrt{s}=29$ GeV in the High Resolution Spectrometer detector. K^0 and charged-particle distributions are compared in a study of the hadronization of quarks of known flavor. Events of the reaction $e^+e^-\rightarrow c\bar{c}$ are tagged by identifying D^*'s while $u\bar{u}$, $d\bar{d}$, or $s\bar{s}$ events are tagged through the identification of a charged particle with fractional momentum near 1. Parton-shower models with cluster and string fragmentation are compared with these data. Also, certain particle scaling tests are performed using the quark-flavor tags. In addition, K^0 production in two- and three-jet events is compared to these models.

I. INTRODUCTION

In this paper we examine particle distributions produced in e^+e^- collisions at a center-of-mass energy of 29 GeV. The experiment was done using the High Resolution Spectrometer (HRS) located at the PEP colliding rings at the Stanford Linear Accelerator Center (SLAC). The strange particle K^0 is used as a probe of the process of hadronization. Throughout this paper we shall refer to the summed K^0 and $\bar{K}^0$ distributions simply as K^0 distributions. The K^0's are easily identified through the $K^0\rightarrow\pi^+\pi^-$ decay and may, therefore, be used as strangeness tags in studying the process of quark hadronization into jets. Section II discusses the specific hadronization models used. These models predict the particle content of the final-state jets; for example, the relative numbers of strange to nonstrange particles are given for each jet flavor. Section III of this paper describes the HRS detector as used in this analysis and presents the K^0-meson cross sections from the full data sample corresponding to an integrated luminosity of 291 pb^{-1}. Approximately 7000 K^0's are contained in this sample. The cross sections are compared with data from other experiments as well as with hadron-fragmentation models.

Section IV describes the flavor-tagging techniques used to identify events originating from a particular $q\bar{q}$ flavor. Events originating as $c\bar{c}$ pairs are tagged by the presence of a D^* meson. The decay of the $D^{*+}\rightarrow D^0+\pi^+$ with the subsequent decays $D^0\rightarrow K^-+\pi^+$, $K^-+\pi^-+\pi^0$, or $K^-+\pi^++\pi^-+\pi^+$ gives a signature with little back-

ground. Rapidity distributions of K^0's and charged particles are then made relative to the direction of the tagging D^*'s. Similarly, a charged particle with fractional momentum $x = p/p_{\text{quark}} > 0.65$ serves as a tag for events originating from a light-quark pair, $u\bar{u}$, $d\bar{d}$, or $s\bar{s}$. The heavier c and b quarks give hadrons that decay into several particles with typically smaller x. The excellent momentum resolution of the HRS makes it possible to select light-quark events in this way. Comparisons are made of K^0 and charged-particle distributions from both tagged samples and the total data set. These data are also compared with phenomenological hadronization models.

Section V examines the characteristics of the charged-particle fragmentation of the low-momentum quarks in the tagged jet. The hadron momenta are scaled to the momentum of the initiating quark rather than the usual 14.5 GeV/c. This allows a direct check of the splitting-function parametrization proposed by Feynman and Field. Section VI presents a brief description of the fragmentation of partons into K^0's for both two jet and multijet events.

II. MODELS OF HADRONIZATION

The gross features of hadronic production in e^+e^- collisions are well understood in the context of QCD. A quark-antiquark pair with large virtuality (or q^2) evolves through a parton shower of quarks and gluons of decreasing virtuality. So long as the parton virtuality is large, α_s is small and the perturbative shower calculations are reliable. In this study we make comparisons with Monte Carlo models which generate coherent or angle-ordered showers where emission angles of successive gluons decrease monotonically.[1] As the shower progresses the angle ordering greatly reduces the available phase space for gluon emission and hence the number of soft gluons. Such parton-shower evolution exhibits a property called preconfinement where neighboring partons in the tree structure form color singlets of a quark, an antiquark, and a number of gluons. The result of the parton-shower calculation is then a number of color-singlet systems with masses considerably larger than typical hadronic masses.

The transition from this partonic intermediate state through the so-called fragmentation process to the observed particles is less well understood and must be parametrized by using data. Several models attempt to describe the transition from the partonic intermediate state to the hadronic final state. In one successful model, the Lund string model,[2] the color-singlet states store energy in a stringlike force field which breaks up through a polarization of the vacuum into quark-antiquark pairs. In a second class of models such as that of Webber and Marchesini,[3] the partonic state continues its parton-shower evolution to still lower q^2 values. At this point light colorless hadronic clusters are formed (color confinement) which subsequently decay into final-state hadrons.

The global structure of events at energies of the SLAC and DESY storage rings PEP and PETRA, such as the number of jets, the acoplanarity, etc., is dominated by the high-q^2 part of the process susceptible to perturbative calculations. The particle composition of the events, on the other hand, is determined by nonperturbative processes that must be parametrized by a specific fragmentation model. For example, the particle composition in cluster models is set by the cluster masses and their subsequent phase-space decay. In string models the particle composition is described by a number of parameters that are put in by hand, such as the strange-quark suppression factor[4] s/u and the frequencies with which different parton flavors are produced in a string decay. In this paper we look for variations in particle composite due to differences in the fragmentation models.

The K^0 meson provides a means of testing certain details of these fragmentation models. The K^0's originate from several mechanisms: They can be produced as first-rank hadrons (i.e., hadrons incorporating the original quark or antiquark) from the fundamental process $e^+e^- \to s\bar{s}$. [See Fig. 1(a).] They also come from the weak decays of first-rank heavy-flavor hadrons from the processes $e^+e^- \to c\bar{c}$ and $e^+e^- \to b\bar{b}$. [See Fig. 1(b).] In addition, K^0's and K^*'s are produced in the fragmentation process of the color singlets arising from the QCD shower. [See Figs. 1(c) and 1(d).] Primary strange mesons, such as K^*'s, decay to the easily identified K^0's.

In the Webber cluster model, the strange-meson production is suppressed relative to lighter mesons by the restricted phase space available. In Lund string fragmentation the strange-meson production rates are governed by the s/u parameter and by the coefficient b in the symmetric splitting function

$$f(z) = \frac{(1-z)^a}{z} e^{-bm^2/z}, \tag{2.1}$$

which determines the probability that a hadron of mass

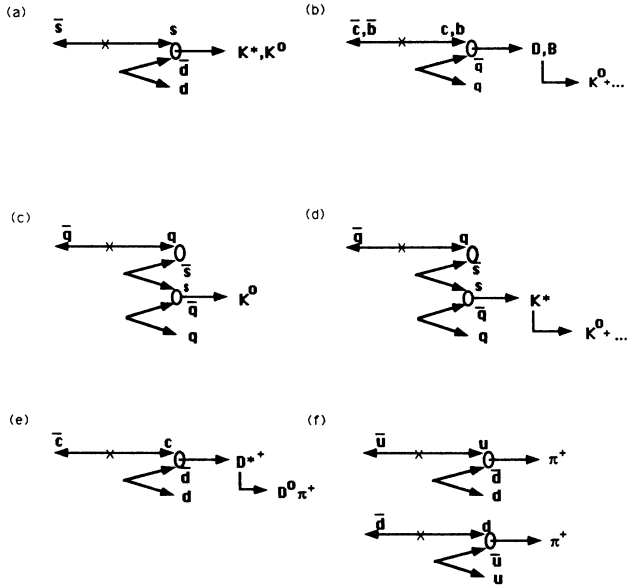

FIG. 1. Quark fragmentation diagrams. (a) First-rank K^* or K^0 production. (b) K^0 production from heavy-flavor decay. (c) Higher-rank primary K^0 production. (d) Higher-rank secondary K^0 production. (e) D^* tagged events. (f) Light-quark tagged events.

m from a fragmenting quark will have energy fraction z of the quark.

We examine both the strange and the nonstrange distributions as a function of the kinematic variables z, the fractional energy, and y, the rapidity, in an attempt to better understand the hadronization process. The ratio of strange to nonstrange particles, for example, depends on the energy density in the color field as viewed in the string models. It is interesting, therefore, to study such quantities in different kinematic regions and for different flavors of hadronizing quarks.

In this experiment we tagged certain classes of events. For example, the primary process, $e^+e^- \to c\bar{c}$ was isolated through the identification of a D^* meson with $z > 0.4$. Since the $c\bar{c}$ production in the fragmentation chain is strongly suppressed by the high c-quark mass, charmed hadrons always come from first-rank particles. We refer to these events as D^* tagged events. Similarly, the $e^+e^- \to u\bar{u}, d\bar{d}, s\bar{s}$ reactions were identified through the existence of one charged particle carrying a majority of the beam momentum.

In a D^{*+} tagged event, such as is shown in Fig. 1(e), not only are the leading quarks identified as c and $\bar{c}$, but also, the measured momentum of the D^{*+} gives the momentum of the unassociated d quark on the tagged side of the event. Knowing the momentum of this d quark (actually, its momentum parallel to the thrust axis), one can examine its fragmentation and compare the results with the 14.5-GeV d-quark fragmentation from the untagged events.

We have also compared the tagged side of the event with the untagged side. The tagging (first-rank) particle is identified and removed before comparing the two sides, and the fragmentation of each side is examined by plotting the ratio of K^0's to total particles on each side of the event. Similarly, the numbers of K^0's from jets of different *flavor* are compared. The total event sample (without tagging) is compared with c quark jets and with light quark jets.

III. EVENT SELECTION AND CROSS-SECTION MEASUREMENTS

The HRS is well suited to the detection of K^0's because of its good mass resolution. The detector has been described in detail elsewhere.[5] Here we simply recall the main features relevant to the present analysis. The tracking of charged particles is performed in a 15-layer drift chamber which extends in radius from 0.2 to 1.1 m. A two-layer outer drift chamber provides additional position measurements at a radius near 2 m. The intrinsic resolution of the chambers of 200 μm, together with the 1.62-T magnetic field, yields a momentum resolution of $\sigma(p_\perp)/p_\perp = 0.002 p_\perp$ (GeV/c). The tracking volume is surrounded by lead-scintillator shower detectors with an energy resolution of $\sigma(E)/E = 0.16/\sqrt{E}$. Hadronic events were selected by requiring that the sum of the visible charged momentum and shower energy in the calorimeters be greater than 10 GeV and that the charged multiplicity be greater than 4. Of the 166 000 events surviving these cuts, approximately 123 000 are hadronic events. The remainder include two-photon and beam-gas events.[6] These cuts effectively remove Bhabha events, muon pairs, and all but a small fraction of tau pairs.

The selection criteria for K^0's were described in detail in a previous paper.[7] These criteria select tracks which clearly originate from a secondary vertex and which combine to give a momentum consistent with a neutral particle from the primary vertex. Figure 2 shows the effective mass plot of pairs of oppositely charged particles interpreted as pions. A narrow peak is seen at the mass of the K^0 over a small combinatoric background. This mass distribution is empirically fit by a Breit-Wigner form plus a linearly falling background as shown by the solid line in Fig. 2. The broad tails arise from K^0 decays where at least one track is less well measured, either because it is not measured in the outer drift chamber, or because its momentum is low. The fit parameters are $M = 496.9$ MeV and $\Gamma = 9.7$ MeV.

For purposes of cross-section determination the background under the K^0 peak was taken to be linear as in the above fit. The signal region used was 478–518 MeV/c^2. In the signal region the background was approximately 10%. The K^0 acceptance was determined using the HRS Monte Carlo,[8] our full detector simulation program. A bin-by-bin acceptance correction was done as a function of the fractional energy, z. The background subtracted, acceptance corrected data were then converted to the scaling cross section, $(s/\beta)d\sigma/dz$ in nb GeV^2, using the known luminosity of 291 ± 7 pb^{-1} and a center-of-mass energy squared corrected for initial-state radiation of $s = (28.3\ \text{GeV})^2$. The measured cross section values from $0.06 < z < 0.70$ are listed in Table I(a) and are plotted in Fig. 3(a). The plotted errors are the quadratically combined statistical and systematic errors on each point.

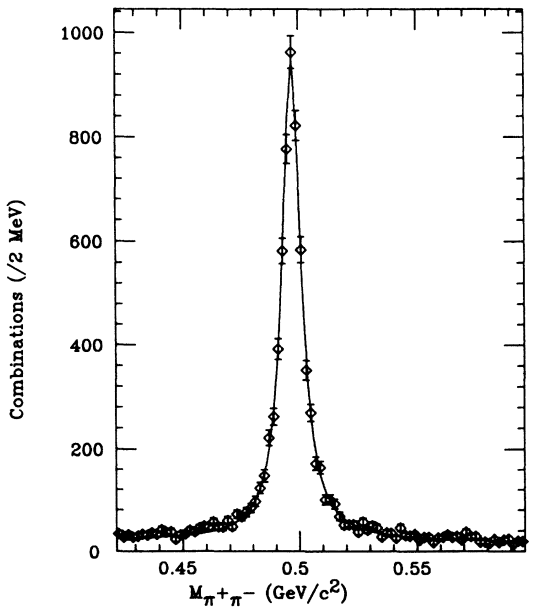

FIG. 2. Effective-mass plot of pairs of oppositely charged particles after selection cuts of Ref. 7. The solid curve is a Breit-Wigner-form-plus-linear-background fit.

Below z of 0.06, background levels are high and the acceptance is rapidly changing.[9] The Lund 6.3 prediction is shown in Fig. 3(a) for comparison. It agrees with these data in both normalization and slope. Figure 3(b) shows the data from this experiment plotted with cross sections measured by TASSO (Ref. 10), TPC (Ref. 11), JADE (Ref. 12), and Mark II (Ref. 13) at nearby center-of-mass energies. There is good overall agreement.

The total cross section for K^0 production is calculated from the sum of acceptance corrected K_S^0's in each z bin.

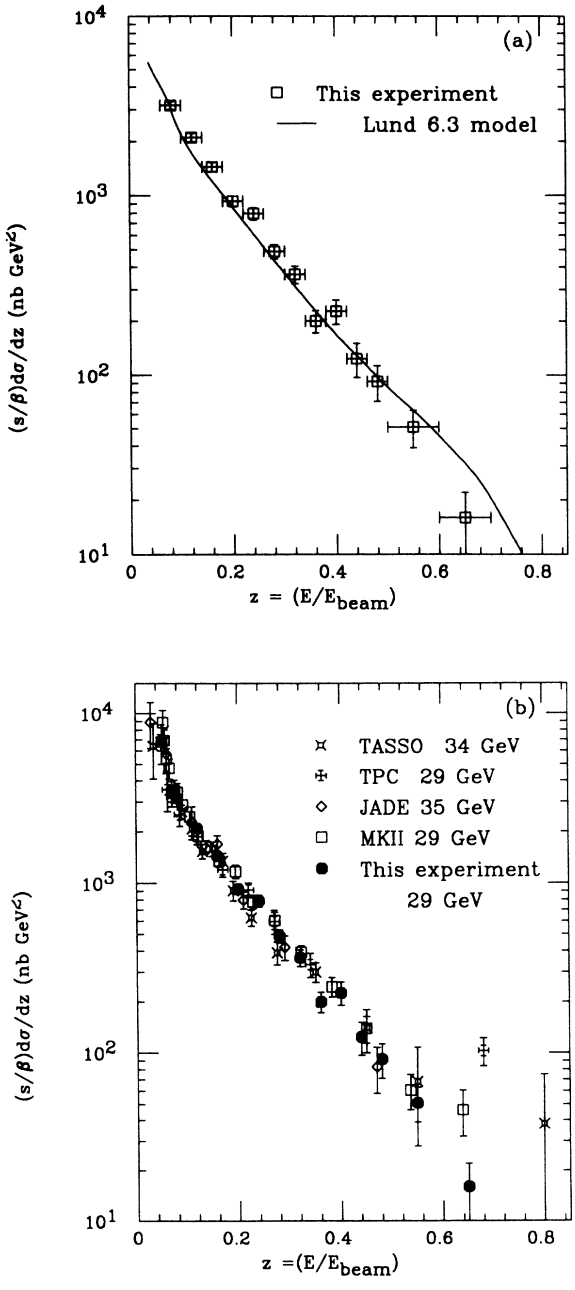

FIG. 3. K^0 scaling cross sections as a function of fractional energy. (a) This experiment with the Lund 6.3 shower-model (Ref. 2) prediction. (b) This experiment with data from TASSO (Ref. 10), TPC (Ref. 11) JADE (Ref 12), and Mark II (Ref. 13).

Approximately 15% of all $\pi^+\pi^-$ decays of the K_S^0 are reconstructed and fall into our fiducial interval, $0.06<z<0.70$. Since only 68.6% of the K_S^0's decay to $\pi^+\pi^-$, our overall detection efficiency for K_S^0's is approximately 10%. Thus, the 7155 observed $K_S^0\to\pi^+\pi^-$ decays scale to $69\,927\pm882\pm1271$ K_S^0's. Taking into account the fact that half of the K^0's decay to K_S^0's, and dividing by the measured luminosity, we find a measured total cross section of

$$\sigma_{K^0}=480.6\pm6.1\pm14.5 \text{ pb} \tag{3.1}$$

in the interval $0.06<z<0.70$. If the Lund Monte Carlo cross-section shape is extrapolated to the unmeasured intervals at either extreme, the total cross section becomes[14]

$$\sigma_{K^0}=613.7\pm7.8\pm38.4 \text{ pb} \tag{3.2}$$

in the interval $0.0<z<1.0$.

From the total cross section the value of the ratio of cross section to the QED cross section $\sigma(e^+e^-\to\mu^+\mu^-)$ can be calculated. Radiative corrections reduce the average center-of-mass energy for the HRS geometry from 29 to 28.3 GeV. Therefore, the R value is given by

$$R_{K^0}(0<z<1.0)=\frac{\sigma_{K^0}(0<z<1.0)}{\sigma_{\mu\mu}(\sqrt{s}=28.3 \text{ GeV})}$$
$$=5.65\pm0.07\pm0.36\ , \tag{3.3}$$

where $\sigma_{\mu\mu}=108.5\pm0.0\pm1.5$ pb. The number of K^0's per event is then given by the ratio of $R_{K^0}/R_{\text{hadronic}}$. Using the total R value[15] of $R_{\text{hadronic}}=3.96\pm0.03\pm0.09$, as measured by the MAC Collaboration, we find that the total number of K^0's per event is

$$\frac{R_{K^0}}{R_{\text{hadronic}}}=1.427\pm0.021\pm0.097\ . \tag{3.4}$$

The number of K^0's per event predicted by the Lund 6.3 Monte Carlo[2] program varies linearly with the parameter s/q and is relatively insensitive to the other Lund parameters. We have previously[16,17] used the HRS production cross sections of K^{*0}, ρ, and D mesons to fit the Lund parameters. The s/q parameter from that fit was 0.34 ± 0.03. The Lund 6.3 model with $s/q=0.30$ (the Lund default value) gives 1.29 ± 0.02 K^0's per event while Lund with $s/q=0.34$ (the HRS fit value) gives 1.38 ± 0.02 K^0's per event, in better agreement with our measured value above.

The Webber cluster model[3] has fewer parameters. The QCD shower is allowed to continue down to a gluon-mass cutoff of order 0.75 GeV. These gluons then decay to $q\bar{q}$ pairs, and colorless combinations of q's and $\bar{q}$'s form clusters with typical masses of a few GeV/c^2. As the gluon cutoff is lowered the cluster masses are reduced, and the probability of the decay of clusters to $s\bar{s}$ pairs decreases as the phase space is reduced. Thus, the cluster models have a natural mechanism for strangeness suppression. As an example of the sensitivity of the number of K^0's per event to the gluon-mass cutoff, changing the cutoff from the default value of 0.75 to 0.65 GeV

reduces the number of K^0's per event from 1.60 ± 0.03 to 1.44 ± 0.03, compatible with our measured value above. The error 0.03 reflects the statistics on the finite number of events generated.

We now turn to a discussion of the K^0 rapidity distribution. The rapidity is defined as $y=0.5\ln(E+p_\parallel)/(E-p_\parallel)$ relative to the event thrust axis, which is calculated using only the charged tracks. Contributions from the decays of first-rank particles tend to cluster at large $|y|$ while particles from the resulting fragmentation chain populate the kinematically available region more uniformly, producing a broad peak near $y=0$.

The K^0 differential cross section as a function of the rapidity, $(1/\sigma_{\text{hadronic}})d\sigma/dy$, is shown in Fig. 4(a). The measured values are given in Table I(b). A broad peak extends out to $|y|$ near 2.0 with a modest but significant dip at $y=0$. Both the string and the cluster models described in Sec. II of this paper predict such a qualitative shape as seen by the predictions of the Lund string model (version 6.3) and the Webber cluster model (version 4.1) shown in Fig. 4(a). The heavy-quark pairs ($b\bar{b}$ and $c\bar{c}$) produce leading hadrons which often decay to K^0's. These K^0's typically have larger rapidity than K^0's from the remainder of the fragmentation, and produce the expected peak in the cross section at large $|y|$. The interference between coherent gluons[18] also suppresses the cross section at small $|y|$. The dip in $d\sigma/dy$ at $y=0$ is more pronounced using the thrust axis than using the sphericity axis.[19] However, a significant dip exists at $y=0$ in both distributions.

Figure 4(b) illustrates the effects of heavy-quark decay by showing the explicit contributions to the differential cross section from $c\bar{c}$ quark pairs and from $u\bar{u}$ quark pairs according to the Lund string model. The $c\bar{c}$ pairs contribute substantially more K^0's at large $|y|$. In Fig. 4(b) the dip near $y=0$ in the K^0 distribution from Monte Carlo $u\bar{u}$ events indicates the magnitude of the coherent gluon interference mentioned above.

The TASSO (Ref. 10) K^0 and the TPC (Ref. 18) $K^\pm$ rapidity distributions are also shown in Fig. 4(a). The three data sets are in close agreement. The Lund string

TABLE I. The K^0 differential cross section as a function of (a) the fractional energy and (b) the rapidity for the total 291-pb^{-1} HRS data.

z	$\frac{s}{\beta}\frac{d\sigma}{dz}$ (nb GeV^2)	z	$\frac{s}{\beta}\frac{d\sigma}{dz}$ (nb GeV^2)
	(a)		
0.08	3156±81±139	0.36	200±17±22
0.12	2099±55±94	0.40	226±18±30
0.16	1445±44±72	0.44	124±15±22
0.20	928±35±53	0.48	92±11±18
0.24	791±34±53	0.55	51±6±10
0.28	488±25±36	0.65	16±4±5
0.32	363±23±34		
y	$\frac{1}{\sigma H}\frac{d\sigma}{dy}$	y	$\frac{1}{\sigma H}\frac{d\sigma}{dy}$
	(b)		
0.125	0.426±0.036	2.125	0.457±0.032
0.375	0.504±0.041	2.375	0.373±0.031
0.625	0.515±0.037	2.625	0.269±0.028
0.875	0.605±0.046	2.875	0.114±0.018
1.125	0.553±0.037	3.125	0.092±0.028
1.375	0.580±0.037	3.375	0.012±0.005
1.625	0.581±0.037	3.625	0.023±0.047
1.875	0.555±0.035		

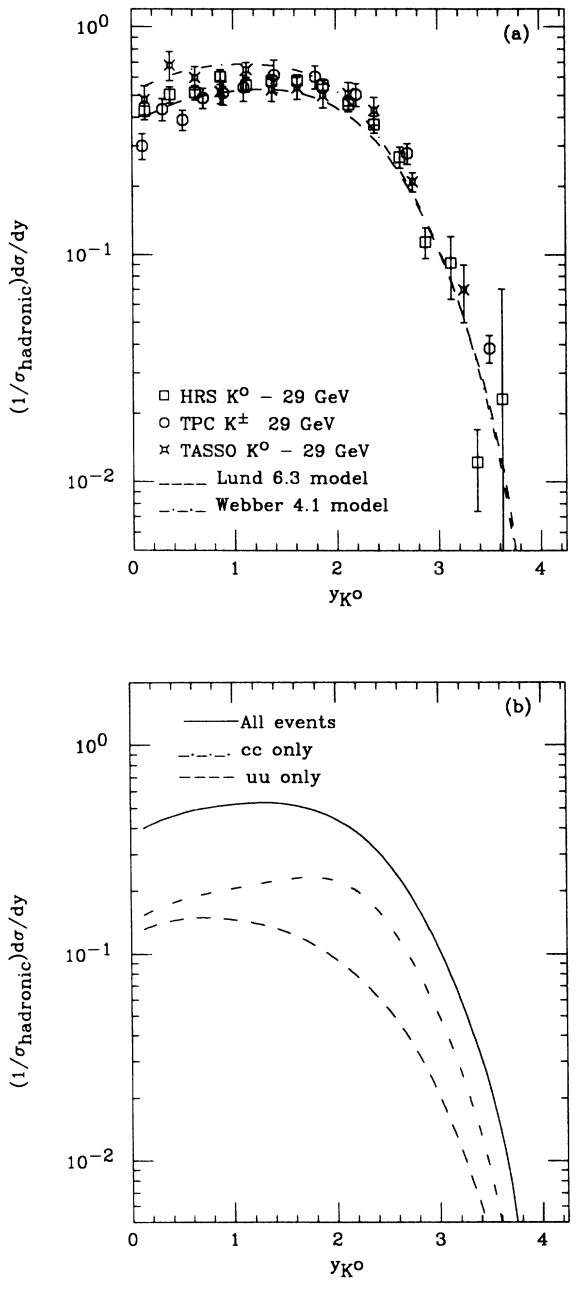

FIG. 4. Normalized K^0 cross sections as a function of rapidity. (a) Lund 6.3 (dashed curve) and Webber 4.1 (dotted-dashed curve). The TPC (Ref. 18) $K^\pm$ data and the TASSO (Ref. 10) K^0 data are shown for comparison. (b) Cross-section breakdown in the Lund 6.3 model.

model in Fig. 4(a) agrees well with these data in both shape and normalization. Though the cluster model gives the correct qualitative features of the data, it predicts a higher rapidity plateau, in disagreement with the measurements presented here.

IV. FLAVOR-TAGGING TECHNIQUES

In a previous publication[20] we have described in detail a technique for the selection of light-quark jets (u,d,s) in e^+e^- collisions. The light-quark sample is obtained by selecting all events with a single charged particle of momentum fraction, $x=2p/\sqrt{s}$ greater than some high value which we choose to be 0.65, corresponding to $p>9.43$ GeV/c. The sample size can be traded off against background contamination by changing the value of this cut. Pions and kaons from heavy-quark decays usually have considerably lower momenta because of the high multiplicities of these decay modes. The estimated background from $c\bar{c}$ and $b\bar{b}$ events is (13±2)%. Of our sample of 859 events, 67% are estimated to be $u\bar{u}$ events, 8% $d\bar{d}$ events, and 12% $s\bar{s}$ events. We shall refer to these events as the light-quark events or the high-x tagged events.

The charm-quark data sample is selected by observation of a $D^{*0}\to D^0\pi^+$ decay where the D^0 decays to either $K^-\pi^+$, $K^-\pi^+\pi^-\pi^+$, or $K^-\pi^+\pi^0$. [See Fig. 1(e).] For the $K\pi$ and $K\pi\pi$ decays of the D^0 the fractional momentum of the D^* was limited to $0.4<z_{D^*}<1.0$, while for the $K\pi\pi\pi$ decays of the D^0 the D^* was limited to $0.6<z_{D^*}<1.0$. The number of events thus selected is 1289. The $b\bar{b}$ events are effectively eliminated by the z cuts on the D^*. The light-quark contamination in this sample is estimated to be[20] (15±3)%. [See Fig. 1(f).] We shall refer to these events as the charm-quark events or as the D^* tagged events.

With these tagged events we compare the fragmentation processes initiated by quarks of different flavor. In our previous study[20] based on approximately one-third of our present data, detailed comparisons between charged-particle distributions were made. Using the full data sample we are now in a position to extend these comparisons and to add K^0 particle distributions to the study.

The three data sets we use are the charm-quark tagged sample, the light-quark tagged sample, and the total data sample. In each case we first extract acceptance corrected distributions for K^0's and for charged particles. Ratios of these distributions show the differences between the role of $s\bar{s}$ pairs in the quark fragmentation chain and the more frequent $u\bar{u}$ and $d\bar{d}$ pairs. Also, by examining both sides of a tagged event we compare high-momentum quark fragmentation with secondary lower-momentum quark fragmentation.

First, we examine the normalized cross section as a function of rapidity for the D^* tagged and the light-quark tagged events. As in the previous rapidity cross section the thrust axis is determined from the charged particles in the event. Here, its direction is taken (arbitrarily) to be in the same hemisphere as the tagging particle. Thus, positive rapidity corresponds to the tagged hemisphere. The observed K^0 distributions are corrected for acceptance by using the rapidity acceptance determined from the total sample. The cross sections are normalized to the hadronic cross section by dividing each distribution by the number of events in the respective tagged samples (1289 D^* tagged events and 859 light-quark tagged events). The cross-section values given in Tables II(a) and II(b) are plotted in Figs. 5(a) and 5(b). In both figures the solid line shows the position of the K^0 cross section for our total data sample, previously plotted in Fig. 4(a).

The heights and widths of the rapidity plateaus are similar for all three distributions. However, by averaging the plateau height over several bins, one notices a lower

TABLE II. The K^0 differential cross section as a function of rapidity for (a) the D^* tagged events and (b) the light-quark tagged events.

y	$\frac{1}{\sigma_H}\frac{d\sigma}{dy}$	y	$\frac{1}{\sigma_H}\frac{d\sigma}{dy}$
	(a) D^* tagged events		
−3.25	0.000±0.081±0.012	0.25	0.081±0.081±0.006
−2.75	0.273±0.137±0.019	0.75	0.466±0.192±0.019
−2.25	0.447±0.155±0.019	1.25	0.428±0.161±0.012
−1.75	0.658±0.199±0.025	1.75	0.416±0.155±0.012
−1.25	0.614±0.192±0.019	2.25	0.391±0.149±0.012
−0.75	0.466±0.192±0.019	2.75	0.205±0.118±0.012
−0.25	0.081±0.081±0.006	3.25	0.161±0.118±0.025
	(b) Light-quark tagged events		
−3.25	0.000±0.121±0.019	0.25	0.242±0.177±0.009
−2.75	0.307±0.177±0.019	0.75	0.354±0.205±0.009
−2.25	0.587±0.224±0.019	1.25	0.363±0.186±0.009
−1.75	0.540±0.224±0.019	1.75	0.447±0.205±0.019
−1.25	0.456±0.205±0.019	2.25	0.000±0.084±0.000
−0.75	0.699±0.289±0.028	2.75	0.000±0.102±0.009
−0.25	0.000±0.121±0.009	3.25	0.000±0.121±0.019

plateau height on the tagged side of each distribution. Since the average energy of the light fragmenting quark on the tagged side is substantially less than the 14.5-GeV quarks of the total data set, we can ask if there is evidence for scaling violation. With scaling, the height of the rapidity plateau would be expected to remain constant as a function of energy of the hadronizing quark. As the quark energy rises the width of the plateau would increase leaving the particle density constant as a function of rapidity. For all charged particles there is definite evidence of nonscaling behavior.[21]. The plateau height is found to rise with energy.

In units of number of K^0's per unit of rapidity, one can compare the nontagged side of the light-quark tagged events (from 14.5-GeV light quarks) with the tagged side of the light-quark tagged or the D^* tagged events (mainly from low-momentum d quarks). The 14.5 GeV light quarks produce a plateau height of 0.546 ± 0.093 to be compared with low-momentum d quarks from the D^* tag of 0.425 ± 0.083, and with low-momentum d quarks from

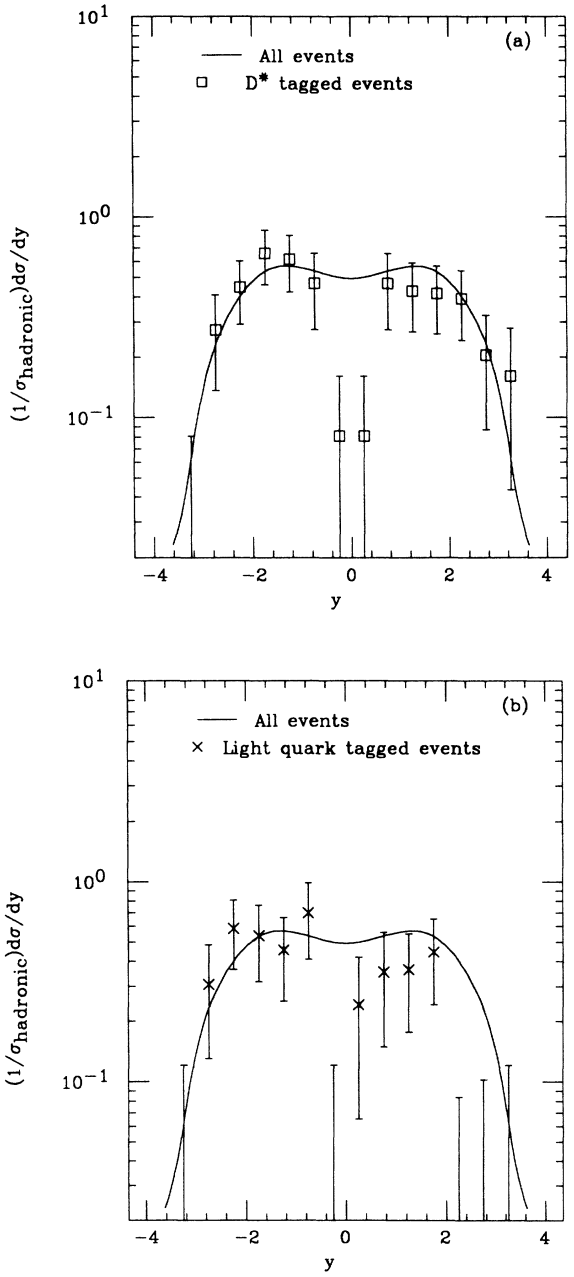

FIG. 5. Normalized K^0 cross section as a function of rapidity. (a) The D^* tagged event sample. (b) The light-quark sample. The solid line in each figure shows the cross section for the total data set.

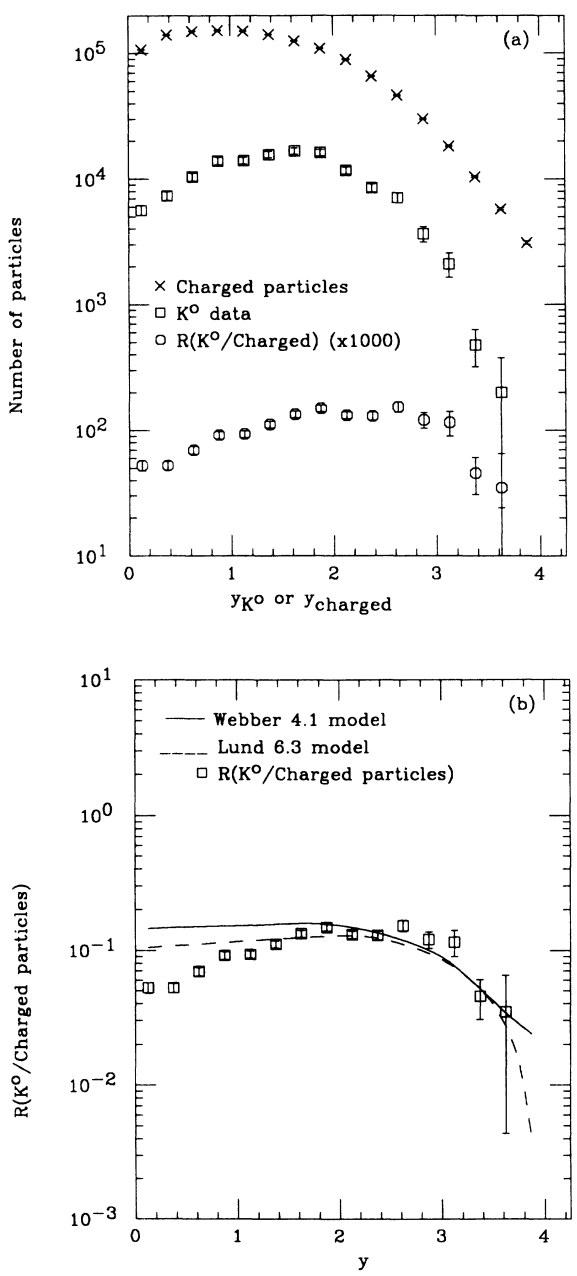

FIG. 6. Rapidity distributions for K^0's, charged particles, and their ratio, $R(K^0/\mathrm{CP})$. (a) The total data set. (b) $R(K^0/\mathrm{CP})$ with the Lund 6.3 model (dashed) and the Webber 4.1 model (solid) predictions.

the light-quark tag of 0.291 ± 0.089. For comparison the total data sample gives a plateau height of 0.528 ± 0.026. In each case an average has been taken over the interval $0.50<|y|<2.50$. Thus, we see evidence of scaling violation from these K^0 distributions.

For the purpose of studying strangeness in our hadronic event sample we define the variable $R(K^0/\mathrm{CP})$ as the ratio of K^0's to charged particles. The value of $R(K^0/\mathrm{CP})$ for the total event sample averaged over all kinematic variables is $0.109\pm0.002\pm0.009$. It is given by the ratio of $1.427\pm0.021\pm0.097$ K^0's per event to $13.1\pm0.05\pm0.60$ charged particles per event,[22] both measured in this experiment. Figure 6(a) shows the rapidity distribution for the charged particles (X), and for the K^0's ($\square$) separately, and for their ratio ($\circ$). Features immediately apparent are a gradual rise in $R(K^0/\mathrm{CP})$ with $|y|$ out to a broad maximum ratio of 0.15 near $|y|=2$, and a falloff for $|y|>3.0$. Also, Fig. 6(b) shows the Lund 6.3 and Webber 4.1 predictions. Both models describe the falloff above 3.0 seen in our data but fail to reproduce the dip at small $|y|$.

Our $c\bar{c}$ events identified by the D^* tag can now be used to examine the charm-quark contribution to $R(K^0/\mathrm{CP})$. The rapidity distribution of $R(K^0/\mathrm{CP})$ is given in Fig. 7(a) for tracks opposite the D^* tag. These tracks come from the fragmentation of a known 14.5-GeV c (or $\bar{c}$)

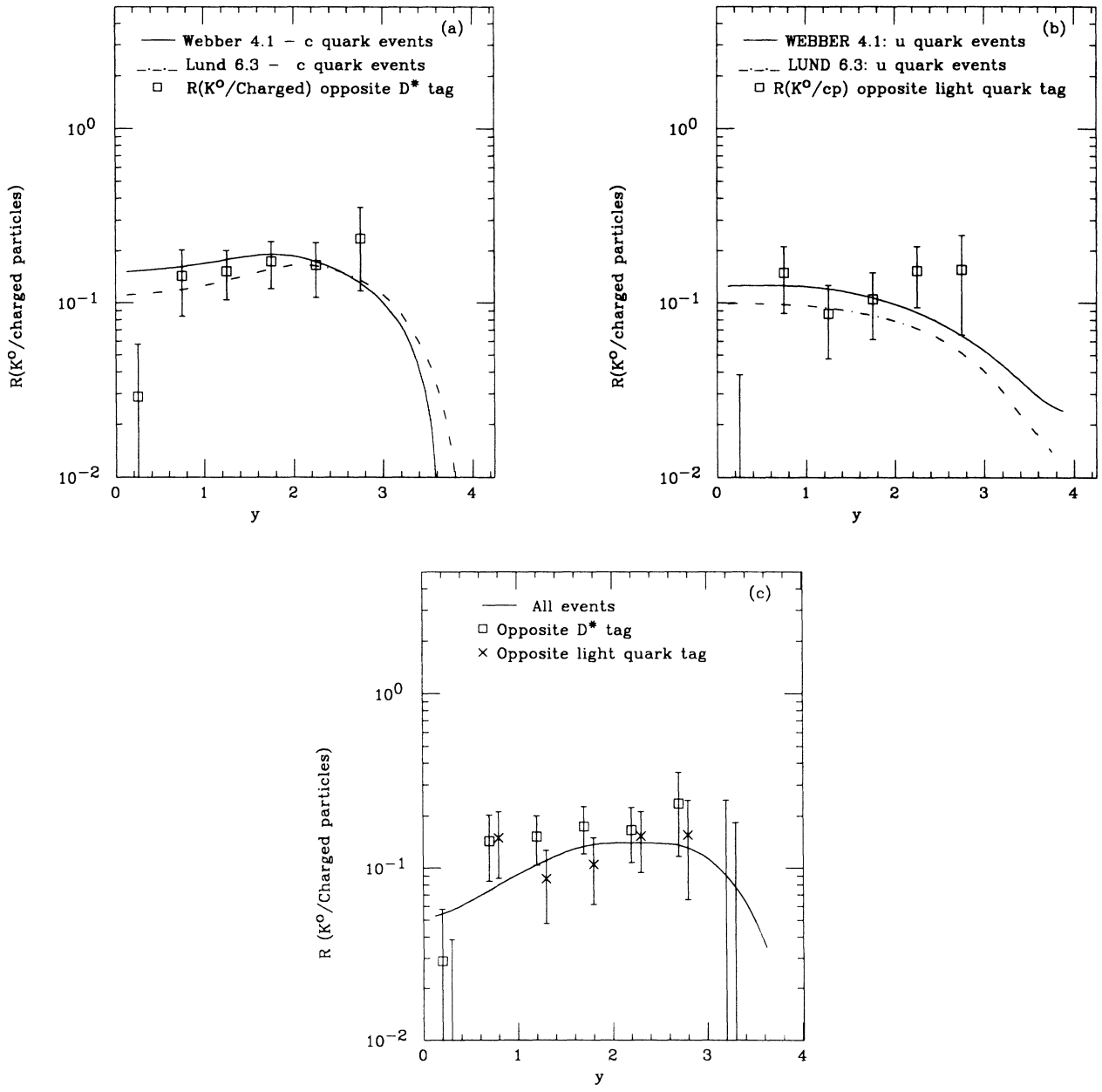

FIG. 7. $R(K^0/\mathrm{CP})$ rapidity distributions. (a) D^* tagged events with the $c\bar{c}$ event predictions of the Lund 6.3 (dotted-dashed) and the Webber 4.1 (solid) models. (b) Light-quark tagged events with the $u\bar{u}$ event predictions of the Lund 6.3 (dotted-dashed) and the Webber 4.1 (solid) models. (c) A comparison of the light-quark tagged events, the D^* tagged events, and the total data set (solid line).

quark and can, therefore, be compared directly with the Lund and Webber ratios from $c\bar{c}$ events alone. These distributions are shown in Fig. 7(a). Since the light-quark tagging enriches the $u\bar{u}$ content of an event sample as described in Sec. II, we compare the ratio $R(K^0/\mathrm{CP})$ for tracks opposite the light-quark tag with the same ratio from Monte Carlo–generated $u\bar{u}$ events. These data and predictions are shown in Fig. 7(b). For both tagged samples Lund and Webber models agree with the data over the full rapidity range. However, our data is not sufficiently precise to separate the two models.

A direct comparison of the three data sets is made in Fig. 7(c). Here $R(K^0/\mathrm{CP})$ is plotted for the total sample (solid line), for the 14.5-GeV c-quark sample (□), and for the 14.5-GeV light-quark sample (X). At the level of statistics of these data the three distributions are indistinguishable.

V. CHARGED-PARTICLE SCALING TESTS

Since we have a relatively clean tagged sample of charm events, where the secondary quark must be a d (or $\bar{d}$) quark, as in Fig. 1(e), we can make certain cross checks of the kinematics of this parton picture. The momentum of this secondary d quark is known from the measured D^* momentum, and its fragmentation properties can be measured. To the extent that the fragmentation of the two original quarks is independent, we check for the scaling behavior of the fragmentation function $[D_\pi^q(z)]$, by comparing $D_\pi^d(z)$ for these lower-momentum d quarks from tagged events with the original 14.5-GeV quarks.

We do this by plotting the charged-particle fractional momentum distribution (z) from several sources. Concentrating first on the light-quark tagged events, we plot in Fig. 8(a) three charged-particle z distributions: those from the total hadronic sample (✦), those in the hemisphere opposite the tag (□), and those in the same hemisphere as the tag (○). For the first two distributions (✦ and □), the shapes are exponential above $z \approx 0.1$ but peak at lower z values. The charged-particle distribution on the tag side (○) coming from the low-momentum d quark is considerably softer, as expected. To check the scaling hypothesis the same particles are plotted after scaling their energies by $z_{\mathrm{new}} = z/\eta$, where $\eta = (1 - p_{\mathrm{high}\ x}/14.5)$ is the fractional momentum of the d quark. This scaled distribution (X) is also shown in Fig. 8(a) and is seen to have the same z distribution as the total hadronic sample and the light-quark untagged hemisphere data. Only in the region $z < 0.1$ does one see a deviation, consistent with previously observed scaling violations.[23] Specifically, at low z the d-quark produced spectrum falls below the 14.5-GeV light-quark produced spectrum, even after renormalizing the d-quark momenta to 14.5 GeV.

Figure 8(b) makes a similar comparison for D^* tagged events. Here also hadrons on the D^* side (○) come from the remaining d quark. When scaled up to 14.5 GeV, the distribution of hadrons (×) is compared directly with the 14.5-GeV c-quark distribution (□). Again we see agreement in slope for the majority of the z range with a deviation at small z, indicating a scaling violation. In summary, we have measured both the hadron momentum spectrum produced by 14.5-GeV quarks and the softer hadron spectrum from low-momentum quarks. A simple linear scaling of the low-momentum hadron by the ratio of quark momenta gives a scaled momentum distribution which compares well with the measured hadrons from 14.5-GeV quarks.

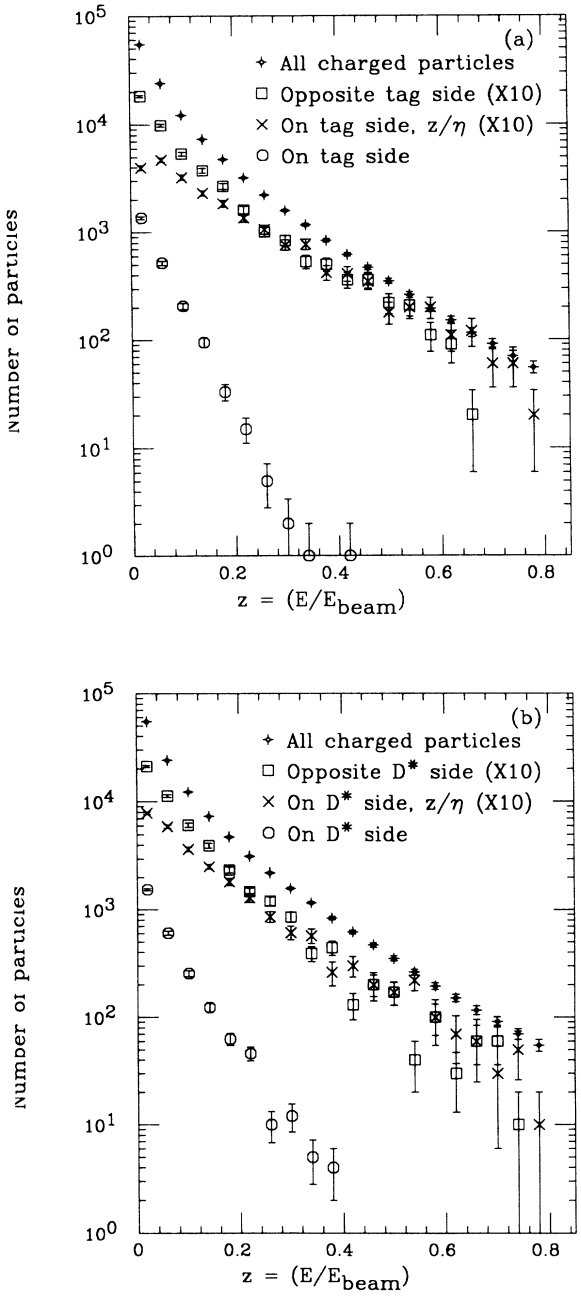

FIG. 8. The charged-particle fractional-energy distributions. (a) The total data set (✦), the hemisphere opposite the D^* tag side scaled to the quark momentum (crosses). (b) The total data set (✦), the hemisphere opposite the light-quark tag (open squares), the hemisphere on the light-quark tag side (open circles), and the hemisphere on the light-quark tag side scaled to the quark momentum (crosses).

Field and Feynman[24] developed a simple parametrization of the properties of quark jets based on the idea that a universal function $[f(\eta)]$ could describe the fragmentation process. Starting with a quark of known momentum, the quark fragments into a hadron of fractional momentum z plus a remaining jet with momentum fraction $\eta=1-z$. The function $f(\eta)$ gives the probability that the remaining jet has a fraction η of the original quark's momentum. In this picture $c\bar{c}$ events produce a D^* plus a d quark of known momentum. By studying the fragmentation of these known d quarks, we can determine $f(\eta)$ directly. The measured quantities are the distributions of primary mesons of flavor h, from a quark q called $D_q^h(z)$.

Field and Feynman show that

$$D_d^{\pi^+}(z)-D_d^{\pi^-}(z)=\gamma f(1-z)=\gamma f(\eta)\ , \tag{5.1}$$

where γ is the probability of $u\bar{u}$ or $d\bar{d}$ quark pair creation. For an $s\bar{s}$ pair creation probability of half of the $u\bar{u}$ or $d\bar{d}$ probability, $\gamma=0.4$. A simple parametrization of $f(\eta)$ was used by Feynman and Field to fit electroproduction data and is

$$f(\eta)=1-a+3a\eta^2 \tag{5.2}$$

with $a=0.88$. To determine the function $f(\eta)$ we first scale the fractional momentum of each particle in the same hemisphere as the D^* tag (excluding the D^* decay particles, as usual) by the fractional momentum of the d quark as follows:

$$z'=\frac{z}{1-P_{D^*}/14.5}\ , \tag{5.3}$$

where z' is the fractional momentum relative to the d-quark momentum. The difference of the positive- and negative-charge distributions is fitted to the function, $f(1-z')$ as in Eq. (5.1) above. As expected for light-quark fragmentation the function $f(1-z')$ is large for large η (small z'). That is, most of the time the remaining quark carries off the majority of the momentum.

A similar analysis is done for the light-quark tagged events where a majority of the events are from $u\bar{u}$ fragmentation and where the remaining quark is also a d (or $\bar{d}$) quark of known momentum. The difference distribution is similar in shape to the D^* tagged distribution. Figure 9 shows the difference distribution $D_d^{\pi^+}-D_d^{\pi^-}$ for the total sample of d quarks from both D^* and light-quark tagged events. The solid line in Fig. 9 shows a fit to $f(1-z')$ with the parameter $a=1.15\pm0.04$. The 14.5-GeV light quarks are identified opposite the light-quark tag. The difference distribution from their fragmentation shows the same behavior and is also well fit by the functional form $f(\eta)$.

VI. TWO- AND THREE-JET EVENTS

In a previous study of HRS data[22] a cut in sphericity of $S\leq0.25$ and in acoplanarity of $A\leq0.10$ was used to define a two-jet event sample. We now compare the relative number of K^0's to charged particles for the two-jet and multiple-jet events. Figure 10 shows these distributions. Notice that while the charged-particle rapidity spectra for two jets and multiple jets differ only slightly, the K^0 spectra are quite different. There is a distinct excess of low rapidity K^0's in the total sample and hence in the multiple-jet sample.

Both the charged particle distributions from the previous study and the K^0 distributions have been corrected

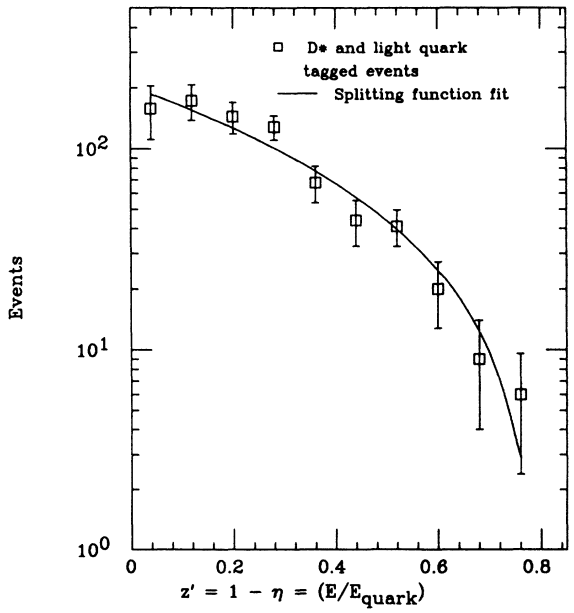

FIG. 9. The Field-Feynman probability function, $f(\eta)=1-a+3a\eta^2$ with $a=1.15\pm0.04$, superimposed on the difference of the distributions, $D_d^{\pi^+}-D_d^{\pi^-}$. See text for definitions.

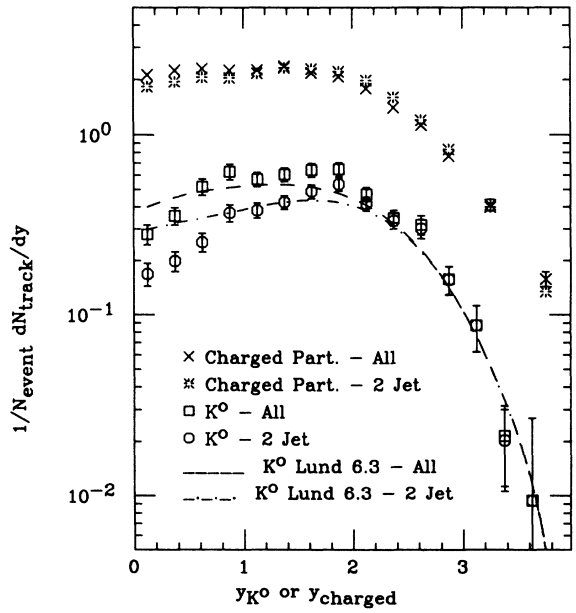

FIG. 10. The K^0 and charged-particle rapidity distributions for two-jet events (selected as described in the text) and for all events. The Lund 6.3 rapidity distribution predictions for two-jet events (dotted-dashed) and for all events (dashed).

for efficiency. The charged-particle distributions have also been corrected for the distortions due to the interpretation of all charged tracks as π mesons.[22] This correction is not needed for the K^0's whose mass is known. The K^0 detection efficiency as a function of rapidity was determined from the HRS Monte Carlo[8] study. The same efficiency function was used to correct both two-jet and multiple-jet events.

One expects more low momentum K^0's in multiple-jet events with higher multiplicity and, hence, lower momentum per particle. Also, the gluon jets found in multiple-jet events are expected to have a higher probability for $s\bar{s}$ pair production than quark jets of comparable energy. We have tested these hypotheses by examining the K^0 distribution as a function of rapidity for Monte Carlo–generated two-jet and multiple-jet events. In agreement with the HRS data, Lund 6.3 (shown in Fig. 10.) and Webber 4.1 show an excess of K^0's near $|y|=0$ for the multiple-jet sample.

VII. CONCLUSIONS

Final K^0 cross sections have been presented for 291 pb^{-1} of data and were compared with measurements at similar energies in e^+e^- scattering. By tagging events we identified hadronic showers coming from quarks of known longitudinal momentum and flavor. The tag identified both a 14.5-GeV quark opposite to the tag and a lower-momentum light quark on the tagged side. For these lower-momentum quarks we found the following.

(a) A simple splitting function described the charged-particle hadronization.

(b) The fractional energy spectrum scaled with the momentum of the quark in a simple way. The ratio $R(K^0/\mathrm{CP})$ for the hadrons produced by charm quarks and light quarks was examined as a function of rapidity. Even with the small number of tagged events in this experiment, there was an indication of a deviation in $R(K^0/\mathrm{CP})$ from both the string- and cluster-model predictions.

The hadronization of quarks of different flavor was studied by comparing the 14.5-GeV quarks opposite the event tags. For these high-momentum quarks, no indication was found in these data of a flavor dependence of the ratio $R(K^0/\mathrm{CP})$ as a function of the kinematic variables examined.

ACKNOWLEDGMENTS

We wish to thank the SLAC cryogenics group and the technical staffs of PEP and the collaborating institutions whose contributions made this experiment possible. This work was supported in part by the U.S. Department of Energy under Contracts Nos. W-31-109-ENG-38 (Argonne National Laboratory), DE-AC02-76ER01112 (University of Michigan), DE-AC03-76SF00098 (Lawrence Berkeley Laboratory), DE-AC02-76ER01428 (Purdue University), and DE-AC02-84ER40125 (Indiana University).

---

[a]Present address: Fermi National Laboratory, Batavia, IL 60510.
[b]Present address: NIKHEF-H, Amsterdam, The Netherlands.
[c]Present address: CRN Division de Hautes Energies, Strasbourg, France.
[d]Present address: Stanford Linear Accelerator Center, Stanford, CA 94305.
[e]Present address: University of Wisconsin, Madison, WI 53706.
[f]Present address: Brandeis University, Waltham, MA 02254.
[g]Present address: University of Kansas, Lawrence, KA 66045.
[h]Present address: Ohio State University, Columbus, OH 43210.
[i]Present address: Virginia Polytechnic Institute and State University, Blacksburg, VA 24061.
[j]Present address: Electronic Data Systems of Canada, Oshawa, Canada.

[1]A recent comparison of these ideas with data is given by W. Hoffman, in *Lepton and Photon Interactions,* proceedings of the International Symposium on Lepton and Photon Interactions at High Energies, Hamburg, West Germany, 1987, edited by R. Rückl and W. Bartel [Nucl. Phys. B (Proc. Suppl.) **3**, 671 (1987)].

[2]T. Sjöstrand, Comput. Phys. Commun. **27**, 243 (1982); **28**, 229 (1983); T. Sjöstrand and M. Bengtsson, *ibid.* **43**, 367 (1987); T. Sjöstrand, *ibid.* **39**, 347 (1986).

[3]G. Marchesini and B. R. Webber, Nucl. Phys. **B238**, 1 (1984); B. R. Webber, *ibid.* **B238**, 492 (1984).

[4]W. Hoffman, in *Proceedings of the International Symposium on Strangeness in Hadronic Matter,* Bad Honnef, Germany, 1987, edited by J. Speth [Nucl. Phys. **A479**, 337c (1988)].

[5]D. Bender *et al.*, Phys. Rev. D **30**, 515 (1984).

[6]C. R. Ng, Ph.D. thesis, Purdue University [Report No. UMI87-29773), 1987. See Fig. 4.1 in thesis.

[7]M. Derrick *et al.*, Phys. Rev. D **35**, 2639 (1987).

[8]The HRS Monte Carlo program used the Lund version 5.3 as multihadron event generator. The resulting particles were passed through the detector simulation and then processed through the same reconstruction programs as the data.

[9]The efficiency calculation was improved since the publication of Ref. 7 by increasing the number of Monte Carlo events and by widening the K^0 mass cuts and corresponding detection efficiency. The present cross section values supersede those given in Ref. 7.

[10]TASSO Collaboration, M. Althoff *et al.*, Z. Phys. C **27**, 27 (1985).

[11]TPC Collaboration, H. Aihara *et al.*, Phys. Rev. Lett. **53**, 2378 (1984).

[12]JADE Collaboration, W. Bartel *et al.*, Z. Phys. C **20**, 187 (1983).

[13]MARK II Collaboration, H. Shellman *et al.*, Phys. Rev. D **31**, 3013 (1985).

[14]In the measured interval, $0.06<z<0.70$, the Lund 6.3 model agrees well with the observed cross section and is chosen here to extrapolate our data into the unmeasured regions. Where Lund 6.3 gives 78.3% of the K^0's in the measured interval,

the Webber 4.1 model gives 74.3%. The difference between the models is treated here as a model-dependent systematic error in quoting the cross section for the interval, $0 < z < 1$.

[15]MAC Collaboration, E. Fernandez *et al.*, Phys. Rev. D **31**, 1537 (1985). The MAC experimental value of R is used here rather than the HRS value because the detector has excellent charged-particle and photon solid-angle coverage, minimizing their model-dependent detector efficiency determination.

[16]M. Derrick *et al.*, Phys. Lett. **158B**, 519 (1985).

[17]M. Derrick *et al.*, Phys. Rev. Lett. **53**, 1971 (1984).

[18]Z. Wolf, thesis, LBL, Report No. LBL-23738, 1987.

[19]L. V. Gribov, E. M. Levin, and M. G. Ryskin, Phys. Rep. **100**, 1 (1983).

[20]P. Kesten *et al.*, Phys. Lett. **161B**, 412 (1985).

[21]G. Kramer, *Theory of Jets in e^+e^- Annihilation* (Tracts in Modern Physics, Vol. 102) (Springer, Berlin, 1984); G. Wolf, in *Fundamental Interactions: Cargèse 1981,* proceedings of the 1981 Cargèse Summer Institute, Cargèse France, 1981, edited by J-L. Basdevant *et al.* (NATO Advanced Study Institutes, Series B: Physics, Vol. 85) (Plenum, New York, 1982).

[22]D. Bender *et al.*, Phys. Rev. D **31**, 1 (1985).

[23]R. Felst, in *Lepton and Photon Interactions at High Energies,* proceedings of the 10th International Symposium, Bonn, Germany, 1981, edited by W. Pfeil (Physics Institute, Bonn University, Bonn, 1981), p. 52.

[24]R. D. Field and R. P. Feynman, Nucl. Phys **B136**, 1 (1968).